

Seasonal Variation in Circulation and Watermass Distribution on the Ross Sea Continental Shelf

K.ASSMANN*, H.H.HELLMER and A.BECKMANN

*Alfred-Wegener-Institute for Polar and Marine Research, Postfach 12 01 61,
27515 Bremerhaven, Federal Republic of Germany*

Abstract

Changes in water mass distribution and horizontal circulation due to seasonal influences on the Ross Sea continental shelf are investigated using a circumpolar numerical model. An anticyclonic circulation cell that extends across the open shelf and into the ice shelf cavity is formed in the model. The increase of the east-west density gradient, caused by the strong brine release in the Ross Sea polynya in winter, results in an intensification of this anticyclonic cell from 1.5 Sv to 2.5 Sv. This supports the idea that the horizontal circulation on the Ross Sea continental shelf is to a large degree thermohaline driven. In addition to a temporal change in the circulation strength, the changes in the density structure lead to complex temporal and spatial variability in the circulation around Ross Island. Due to seasonal variation in circulation strength and water temperatures, the area averaged basal melt rate of 25 cm/a shows a bimodal seasonal cycle with peaks of 27.5 cm/a in March and 28.5 cm/a in August.

Keywords:

Ross Sea, numerical model, seasonal cycle, water mass distribution, circulation

1 Introduction

The summer waters on the Ross Sea continental shelf are among the best sampled around Antarctica. This is due to the fact that the Ross Sea is ice-free during summer and hence conditions are logistically convenient to conduct oceanographic measurements. However, very little data are available representing conditions in winter and underneath the Ross Ice Shelf. But it is during this time and in this location that modification processes and water mass formation resulting in products that have the potential to form Antarctic Bottom Water take place. The relevant water masses are High Salinity Shelf Water (HSSW) formed in the southwestern Ross Sea during winter due to extensive brine release in the Ross Sea polynya (Zwally et al. 1985 , Jacobs & Giulivi 1998) and Ice Shelf Water (ISW) that forms by means of melting at the Ross Ice Shelf base (Jacobs et al. 1985).

To improve knowledge of the circulation and water mass distribution a numerical model should be a useful tool. Previous modelling efforts concentrated either on the cavity (e.g., Hellmer & Jacobs 1995) or on reproducing the regional shelf circulation over short time periods (e.g., Commodari and Pierini 1999, Bergamasco et al. 1999). We use a coupled sea ice-ice shelf-ocean model configured for the cavity, continental shelf and deep ocean and integrate it for multiple years to obtain a climatologically representative seasonal cycle. Thereby we represent the main component of seasonal forcing, namely, the brine release and freshwater input due to, respectively, sea ice growth and melting, as well as the slope current as the northern boundary of the shelf regime.

2 Model Description

The coupled sea ice-ice shelf-ocean model employed here has been successfully applied to the Weddell Sea in the framework of the BRIOS (Bremerhaven Regional Ice Ocean Simulations) group (Timmermann et al. 2002 a, b). The ocean component is based on the S-coordinate Primitive Equation Model SPEM (Haidvogel et al. 1991), and the sea ice component on a dynamic-thermodynamic sea ice model with a viscous-plastic rheology (Hibler 1979). The interaction between ice shelf base and ocean is described by the same formalism as the one between sea ice and ocean. Therefore the freezing point temperature is calculated as a function of pressure and salinity over the whole model domain. Ice shelf extent and thickness are prescribed as constant over time, and velocities are set to zero (Timmermann et al. 2002 a). The model is run on a circumpolar grid with zonal boundaries at 50°S and 82°S, with an isotropic resolution of 1.5° zonally and 1.5° cos(ϕ) meridionally for the whole circumpolar domain (Fig. 1a), and 24 vertical levels with increasing resolution near ocean surface and bottom. Since the vertical coordinates are terrain-following, the uppermost model layer represents sea surface conditions outside the ice shelf cavity and follows the ice shelf base inside the cavity (Fig. 1b). The bottom topography was prescribed from Smith and Sandwell (1997) north of 70°S, while south of 70°S where the former data set does not extend to ETOPO5 data were used. Ice shelf and water column thicknesses for the Ross Ice Shelf were supplied by Greischar et al. (1992 (electronic version supplied by Greischar)). Since the southern model boundary is located at 82°S, only 80 % of the area of the Ross Ice shelf is represented in the model. However, because much of the area South of 82°S has water column thicknesses of less than 200m (Greischar & Bentley 1980),but the model requires a minimum water column thickness of 200m, inclusion of this area might lead to artefacts in circulation and melt rate. The hydrographic data for initialisation and boundary restoring were taken from the WOCE Hydrographic Programme Special Analysis Centre (Gouretski et al. 1999). As atmospheric forcing, daily NCEP Reanalyses for 10m wind speed, 2m air temperature, specific humidity, cloudiness and precipitation (P-E) were used for the period from 1978 to 1997. The first ten-year period served as a model spin-up time; the following decade (1988-1997) was analysed, and the results shown here represent the mean seasonal cycle over this time period.

3 Model Validation

3.1 θ/S -Characteristics

Comparing the mean modelled θ/S characteristics on the Ross Sea continental shelf for February(summer) and September(winter), the peak salinity of the High Salinity Shelf Water (HSSW)

clearly shows the strong brine input to the water column due to sea ice formation by rising from 34.85 in February to 35.0 in September (Fig. 2 a & b). The summer value lies within the range observed over a 33-year period in the vicinity of Ross Island (Jacobs & Giulivi 1998). Ice Shelf Water (ISW) found on the continental shelf has salinities around 34.7 and minimum temperatures reaching down to -2.2°C (Fig. 2 a & b), values which agree well with observations (Jacobs & Giulivi 1998, Gouretski 1999). Waters in the cavity cluster around the melting line determined by the pressure dependence of the freezing point for seawater at the ice shelf base. A seasonal signal can also be seen in the minimum temperature of the Low Salinity Shelf Water (LSSW). While this is near the winter surface freezing point at -1.85°C in September (Fig. 2 b) it rises to -1.6°C in February (Fig. 2 a) when most of the sea ice has melted and surface waters are heated by increased solar radiation. The characteristic salinity of the Modified Circumpolar Deep Water (MCDW) at just over 34.7 is well-preserved in the model. The temperature maximum is slightly lower (0.6°C) than observed (0.9°C) but still well within range (Jacobs & Giulivi 1998).

3.2 Climatological Annual Mean Circulation

The most striking feature of the horizontal circulation on the continental shelf is the bottom-intensified westward slope current (Fig. 3). In the bottom model layer, modelled velocities in this current are about 7 cm/s in a north-northwestward direction. This compares well with a value of 9 cm/s observed close to the bottom near the continental shelf break in this region (Picco et al. 1999). This current forms in part the northern limb of an anticyclonic circulation cell that extends underneath the ice shelf all the way to the southern model boundary (Fig. 3a). In the surface layer the coastal current splits at 175°W to follow either the ice shelf edge up to Ross Island (Pillsbury & Jacobs 1985, Keys et al. 1990) or the continental shelf break (Fig. 3b). At the bottom and at middepth on the western shelf the flow is guided topographically entering the cavity through McMurdo Sound (Fig. 3a), in agreement with observations (Lewis & Perkin 1985, Locarnini 1994) and the circulation pattern suggested by Locarnini (1994). In the upper ocean, the main flow into the ice shelf cavity is located east of Ross Island. Velocities are directed more to the west in the surface layer than in the bottom layer due to wind influence (Fig. 3b).

In the ice shelf cavity, the anticyclonic circulation is largely confined to the area of larger water column thicknesses west of 175°W . While current velocities of about 3-4 cm/s can be found along the main path, they do not exceed 1.5 cm/s in the eastern cavity. As described by Hellmer & Jacobs (1995), another weak anticyclonic circulation cell can be discerned near the bottom around Roosevelt Island (Fig. 3a). There are two regions in the model where ISW flows out of the cavity: one in the central Ross Sea and one east of Roosevelt Island, both in agreement with Jacobs et al. (1970). The central outflow is located at 173°W , in agreement with the ISW observations by Pillsbury & Jacobs (1985) and Picco et al. (1999). However, in the model this outflow is very weak since the main current follows the sub-ice topography to the east just south of the ice shelf front (Fig. 3a). This is caused by a model resolution (40 km at the ice shelf front) too coarse to represent the north-south

running ridges in this area. The northwestward directed outflow east of Roosevelt Island agrees well with observations (Hellmer & Jacobs 1995, Rock 1995), though the model slightly underestimates bottom velocities with 6 cm/s compared to an observed 9 cm/s (Rock 1995).

3.3 Sea Ice & the Ross Sea Polynya

The Ross Sea polynya is a well-described feature in the sea ice characteristics of the Ross Sea (Zwally et al. 1985, Jacobs & Comiso 1989). Therefore, its representation by the model can be used for additional validation of the coupled sea ice-ocean model. The modelled mean sea ice thickness distribution for September shows reduced values (< 0.7 m) in the southwestern Ross Sea (Fig. 4a) where the polynya has been permanently observed (Jacobs & Comiso 1989). The sea ice drift is directed to the north in the polynya area with velocities up to 15 cm/s (Fig. 4a) due to strong, predominantly southerly winds in the western Ross Sea. Strong, persistent off-shore winds (Fig. 4b) in combination with a thermally homogenized water column in this area suggest that the polynya can be characterized as a latent heat polynya. In the eastern Ross Sea wind velocities are considerably lower and form a quasi-cyclonic feature (see also Jacobs & Comiso 1989). Consequently, with the sea ice much less divergent, a tongue of thick sea ice (> 1.5 m) extends into the central Ross Sea, in agreement with observations by Zwally et al. (1985).

4 The Seasonal Cycle

4.1 Water Mass Distribution and Horizontal Circulation

The summer salinity structure along the ice shelf edge displays the characteristic distribution of predominantly LSSW in the eastern and HSSW in the western Ross Sea (Fig. 5a). The density gradient caused by this salinity structure supports the anticyclonic circulation described in the previous section. A drastic steepening of the isohalines (and isopycnals) occurs in winter because of an enhanced sea ice growth in the Ross Sea polynya (Fig. 5b). Through deep convection the released brine raises the salinity on the western shelf to a value > 34.8 , constant over the entire water column. This enhanced horizontal density gradient increases the circulation strength of the anticyclonic cell from 1.5 Sv in March to 2.5 Sv in November (Fig. 6). This agrees well with the notion that the circulation is strongly controlled by the thermohaline structure on the shelf (Pillsbury & Jacobs 1985). The winter salinity distribution reflects that very different sea ice growth rates exist in the eastern and western Ross Sea. To the east, sea ice formation stays fairly constant around 2 cm/d between April and October, while, to the west, sea ice growth rates vary between 4 and 12 cm/d reaching the maximum in August (Fig.4b).

Considering the vertically integrated transport stream function, the modelled circulation pattern on the Ross sea continental shelf is dominated by an anticyclonic circulation cell that extends from the shelf break to the southern model boundary inside the ice shelf cavity (Fig.6). While this pattern stays the same in the eastern Ross Sea and in most of the cavity throughout the year with variation only in the strength of this circulation cell, more substantial temporal and spatial changes occur around Ross Island. By July, the water column has homogenised at salinities between 34.8 and 34.9 from Ross Island to the Victoria Land coast (Fig. 5b). Through McMurdo Sound HSSW flows south into the cavity over most of the water column (Fig. 5d). Due to the increase in the east-west density gradient, the strength of the anticyclonic circulation cell has increased to 2.3 Sv, i.e., almost to maximum strength (Fig. 7). A northward current of low-salinity water exists all winter along the western slope of McMurdo Sound carrying glacial meltwater out of the cavity (Fig. 5d). This current which rises toward the surface along the ice shelf front carries meltwater out of the cavity all winter. During the peak strength of the circulation (October and November) this current pattern is visible as a small cyclonic circulation of 0.3 Sv south of McMurdo Sound (Fig. 6a) agreeing well with observations made during this time of the year (Barry & Dayton 1988). After sea ice growth has reached its peak in August (not shown), the brine input to the water column in the western Ross Sea starts to decrease. By November, the meltwater flow through McMurdo Sound has been sufficient to erode most of the HSSW near the Victoria Land reversing the zonal density gradient. This in turn supports the northward current and due to a positive feedback increases it. Together with the input of freshwater due to sea ice melting at the surface this process leaves a dome of HSSW at about 170°E (Jacobs & Giulivi 1998) that can be seen in the summer sections (Fig. 5a). During the summer months the minimum depth reached by the top of the dome, here defined as the minimum depth reached by the 34.8 psu isohaline, increases from 100 m in December to 350 m in April. In a sensitivity study with McMurdo Sound closed, the summer horizontal gradient towards lower densities near the Victoria Land coast disappeared (not shown). Therefore, a considerable outflow from the cavity through McMurdo Sound seen in the standard run (Fig. 5d) seems to be necessary to lower salinities in the western Ross Sea sufficiently for the observed dome of HSSW to appear.

The minimum strength of the anticyclonic circulation cell in March and April (1.5 Sv) coincides with the period at which freshwater input due to the melting of sea ice has reduced the horizontal density gradient to its minimum value (Fig.5a). Due to southeasterly winds acting on the ocean surface unperturbed by sea ice in summer, the near-surface inflow east of Ross Island reaches its maximum strength (Fig. 5c). This inflow carries near-surface waters into the ice shelf cavity, only slightly blocked by the shallow ice shelf draft of about 80m (Fig. 5 c & d). The resulting positive meridional density gradient induces a westward current that transports the low-salinity water towards McMurdo Sound along the southern periphery of Ross Island. In the far southwestern corner of the Ross Sea, sea ice growth has already commenced again. The resulting brine release is not yet strong enough to trigger deep convection. Therefore outflow through McMurdo Sound continues to alter the density structure. The vertically integrated transport of this cyclonic circulation around Ross Island amounts to 0.3 Sv (Fig. 7b).

4.2 Melting and Freezing at the Ice Shelf Base

Since previous estimates of the average basal melt rate only include the inner ice shelf cavity and exclude melting of the ice shelf front (Jacobs et al. 1992, Jacobs et al. 1979), the first row of grid boxes defined as ice shelf were not taken into account to calculate a comparable value from the model results. Modelled average melting is 25 cm/a which agrees very well with values previously calculated from measurements, 25 cm/a (Jacobs et al. 1979) and 22 cm/a (Jacobs et al. 1992). A bimodal seasonal cycle exists with maxima in March and August and minima in May and December (Fig. 7).

The March maximum of 27.5 cm/a is caused by warm summer surface waters carried into the cavity with the surface intensified inflow east of Ross Island (Fig. 5c) enhancing the melting south of Ross Island which is already very high (Bamber & Bentley 1994). The thin ice shelf edge in this area might be a result of this warm near-surface inflow. When the circulation strength is above 90 % of its maximum value in August (Fig. 8c), the increased ventilation of the cavity results in a second maximum of melting of 28.5 cm/a. For the May minimum of 24.5 cm/a neither of the mechanisms mentioned above apply: the surface waters have already cooled down and circulation strength is still reduced. After November the mean temperature of the water in contact with the inner ice shelf base drops since cold winter waters have reached this part of the cavity (Fig. 7). With less potential heat for melting the water becomes in situ supercooled as it rises from the southwestern corner towards the centre of the cavity. A large area over which freezing occurs appears in the central cavity (Fig. 8b) where maximum melting rates do not exceed 10 cm/a during the rest of the year. Hence, a second minimum of 20.5 cm/a results for December (Fig. 7). During most of the year freezing at the ice shelf base only occurs in patches at a mean rate of 2.5 cm/a (Fig. 8a & c). Previous estimates of basal freezing rates range from 1 cm/a (Clough & Hansen 1979) to 3.5 cm/a (Jacobs et al. 1979). Between November and February, this rate increases to 7 cm/a in the model's central cavity.

5 Discussion and Conclusions

Validation against summer observations shows that the coupled sea ice-ocean model BRIOS2.2 provides a very reasonable representation of the water mass distribution and the circulation on the Ross Sea continental shelf. The main water mass characteristics are reproduced and the modelled circulation pattern agrees well with observations. In addition, the mass fluxes at the ice shelf base are in the range provided by literature.

The strength of the anticyclonic circulation cell increases from 1.5 Sv in summer to 2.5 Sv in winter accompanied by a shift of the main cavity inflow from east of Ross Island to McMurdo Sound (west of Ross Island). Since the east-west density gradient across the continental shelf steepens drastically in winter due to strong brine release in the Ross Sea polynya, the shelf circulation seems to be pre-

dominantly thermohaline-driven (Pillsbury & Jacobs 1985). Wind does affect the surface circulation, but mostly in summer when the continental shelf is ice-free. During winter, the period of vigorous sea ice production in the Ross Sea polynya and resulting deep convection, surface currents mainly coincide with the subsurface circulation pattern which is controlled by bottom topography.

After the water column has homogenised at high salinities in winter, the main inflow to the cavity is located in McMurdo Sound extending almost over the entire water column. Due to an enhanced ventilation of the cavity caused by higher sub-ice velocities, the averaged basal melt rate reaches a maximum of 28.5 cm/a. During this time a northward, near-surface flow of meltwater from the ice shelf cavity forms in the western McMurdo Sound. A sensitivity study in which McMurdo Sound was closed shows that this current is essential in creating the HSSW dome observed in the western Ross Sea in summer. Not only were higher salinities found near the Victoria Land coast throughout the year in this case, but the absence of the meltwater also leads to an increase in temperature. This results in a decrease of sea ice growth by 10% and, hence, brine input. The fact that despite this reduction the salinities in the western Ross Sea are still higher for a closed McMurdo Sound indicates how important the meltwater current along Victoria Land is for the watermass structure in the western Ross Sea. The positive zonal density gradient for the open case has been enhanced the outflow and weakens the inflow through McMurdo Sound. This and the stronger wind influence at the surface in summer shift the main inflow to the east of Ross Island and closer to the surface. Since this favours the flow of warm near-surface waters into the cavity, the increase in basal melt in the inflow region causes the summer peak of 27.5 cm/a in the overall melt rate. The surface inflow is also responsible for the region of high basal melt rates south of Ross Island as found also by Bamber & Bentley (1994).

The existence of a bimodal signal in a system that can be assumed to be dominated by a strong annual cycle seems at first surprising. However, evidence for this can be found in current measurements along the ice shelf edge near Roosevelt Island (Hellmer & Jacobs 1995) and in the central Ross Sea (Jacobs & Giulivi 1998). Model results by Holland et al. 2003 also confirm the existence of a semiannual mode in circulation strength and basal melting even though the mean melt rate produced by this model is much lower than values found in literature.

The smoothed model topography does not permit the observed in- and outflow pattern along the central part of the Ross Ice Shelf edge (Pillsbury & Jacobs 1985) to develop. The intrusion of weakly modified HSSW into the eastern Ross Sea caused by a single anticyclonic circulation cell supports the idea put forward by Locarnini (1994) that two separate anticyclonic circulation cells have to exist on the Ross Sea continental shelf to preserve the observed horizontal salinity gradient along the bottom. Therefore, the use of a more accurate topography in this area could further improve our results.

The fresh-water budget of the Ross Sea is dominated by the flux due to sea ice production and melting (Fig.9). The fresh-water export due to sea ice transport off the continental shelf is equivalent to 31.7 mSv ($1 \text{ mSv} = 10^3 \text{ m}^3 \text{ s}^{-1}$) which is similar in magnitude to the value calculated by Timmer-

mann et al. (2001) for the inner Weddell Sea. Since the area defined by Timmermann et al. (2001) is considerably larger than that of the Ross Sea continental shelf, this emphasizes the exceptionally vigorous sea ice production in the southern Ross Sea. Ice shelf melting including melting at the ice shelf edge and net precipitation contribute similar amounts of fresh-water with 5.3 mSv and 5.1 mSv, respectively. Since the southernmost part of the ice shelf is not included in the model the fresh-water flux due to ice shelf melting is probably somewhat too small. However, the discrepancy should not be too grave since ice cores taken in this region of the ice shelf show the existence of marine ice and hence basal freezing (Zotikov & Jacobs 1985). As pointed out by Jacobs et al. (2002) the fresh-water fluxes due to ice shelf melting and net precipitation do not balance the fresh-water extracted due to sea ice production. Possible components to balance the budget are sea ice imported from the Amundsen Sea and fresh-water advected with the coastal current.

The general agreement with observations documents that the model is a sound working tool for the Ross Sea environment. Furthermore, this study constitutes a basis for further investigations in the area as well as providing useful insight into the winter processes on the Ross Sea continental shelf.

Acknowledgements

Special thanks go to Ralph Timmermann for the use of his model code and patient help with any problems. The NCEP atmospheric forcing fields were received via the NOAA-CIRES Climate Diagnostics Centre, Boulder, Colorado, using the Web site <http://www.cdc.noaa.gov/>. The authors would also like to thank the reviewers, Ricardo Locarnini and one anonymous, and the guest editor, S.S.Jacobs, for their helpful comments and suggestions.

References

- BAMBER, J. & BENTLEY, C.R. 1994. A comparison of satellite-altimetry and ice-thickness measurements of the Ross Ice Shelf. *Antarctica, Journal of Glaciology*, **20**, 357-364.
- BARRY, J.P. & DAYTON, P.K. 1988. Current patterns in McMurdo Sound, Antarctica and their relationship to local biotic communities. *Polar Biology*, **8**, 367-376.
- BERGAMASCO, A., CARNIEL, S. & CALDESI VALERI, L. 1999. Reconstructing the general circulation of the Ross Sea (Antarctica) using a robust diagnostic model. In SPEZIE, G. & MANZELLA, G.M.R. eds. *Oceanography of the Ross Sea*. Milano: Springer-Verlag, 119-134.
- CLOUGH, J.W. & HANSEN, B.L. 1979. The Ross Ice Shelf Project. *Science*, **203**, 433-434.
- COMMODARI, V. & PIERINI, S. 1999. A wind and boundary driven circulation model of the Ross Sea. In SPEZIE, G. & MANZELLA, G.M.R. eds. *Oceanography of the Ross Sea*. Milano: Springer-Verlag, 135-144.
- GOURETSKI, V., JANCKE, K., REID, J., SWIFT, J., RHINES, P., SCHLITZER, R. & YASHAYAEV, I. 1999. *WOCE Hydrographic Programme Special Analysis Centre*, Atlas of Ocean Sections CD-ROM.
- GOURETSKI, V.V. 1999. The Large-Scale thermohaline Structure of the Ross Gyre. In SPEZIE, G. & MANZELLA, G.M.R. eds. *Oceanography of the Ross Sea*. Milano: Springer-Verlag, 77-102.
- GREISCHAR, L.L., BENTLEY, C.R. & WHITING, L.R. 1992. An analysis of gravity measurements on the Ross Ice Shelf, Antarctica. In ELLIOT, D.H. ed. *Contributions to Antarctic Research III*, Antarctic Research Series Vol. 57, American Geophysical Union, Washington D. C., 105-155.
- GREISCHAR, L.L. & BENTLEY, C.R. 1980. Isostatic Equilibrium grounding line between the West Antarctic inland ice Sheet and the Ross Ice Shelf, *Nature*, **283**, 651-654.
- HAIDVOGEL, D.B., WILKIN, J.L. & YOUNG, R.E. 1991. A semi-spectral primitive equation ocean circulation model using vertical sigma and orthogonal curvilinear horizontal coordinates. *Journal of Computational Physics*, **94**, 151-185.
- HELLMER, H.H. & JACOBS, S.S. 1995. Seasonal circulation under the eastern Ross Ice Shelf, Antarctica. *Journal of Geophysical Research*, **100(C6)**, 10873-10885.
- HIBLER, W.D., III 1979. A dynamic-thermodynamic sea ice model. *Journal of Physical Oceanog-*

raphy, **9(4)**, 815-846.

HOLLAND, D.M., JACOBS, S.S. & JENKINS, A. 2003. Modeling the ocean circulation beneath the Ross Ice Shelf. [this volume]

JACOBS, S.S., AMOS, A.F. & BRUCHHAUSEN, P.M. 1970. Ross sea oceanography and Antarctic Bottom Water formation. *Deep-Sea Research*, **17**, 935-962.

JACOBS, S.S., GORDON, A.L. & ARDAI, J.L.jr. 1979. Circulation and melting beneath the Ross Ice Shelf. *Science*, **203**, 439-443.

JACOBS, S.S., FAIRBANKS, R.G. & HORIBE, Y. 1985. Origin and Evolution of water masses near the Antarctic continental margin: Evidence from $H^2_{18}O / H^2_{16}O$ ratios in seawater. In JACOBS, S.S. ed. *Oceanology of the Antarctic Continental Shelf*, Antarctic Research Series, **43**, 59-95.

JACOBS, S.S. & COMISO, J.C. 1989. Sea Ice and Oceanic Processes on the Ross Sea Continental Shelf. *Journal of Geophysical Research*, **94(C12)**, 18195-18211.

JACOBS, S.S., HELLMER, H.H., DOAKE, C.S.M., JENKINS, A. & FROLICH, R.M. 1992. Melting of ice shelves and the mass balance of Antarctica. *Journal of Glaciology*, **38(130)**, 375-387.

JACOBS, S.S. & GIULIVI, C.F. 1998. Interannual ocean and Sea Ice Variability in the Ross Sea. In JACOBS, S.S & WEISS, R.F. eds. *Ocean, Ice, Atmosphere: Interactions at the Antarctic Continental Margin*, Antarctic Research Series, **75**, 135-150.

JACOBS, S.S., GIULIVI, C.F. & P.A.MELE 2002. Freshening of the Ross Sea during the late 20th century, *Science*, **297**, 386-389.

KEYS, H.J.R., JACOBS, S.S. & BARNETT, D. 1990. The calving and drift of iceberg B-9 in the Ross Sea. Antarctica. *Antarctic Science*, **2(3)**, 243-257.

LEWIS, E.L. & PERKIN, R.G. 1985. The winter oceanography of McMurdo Sound, Antarctica. In JACOBS, S.S. ed *Oceanology of the Antarctic Continental Shelf*, Antarctic Research Series, **43**, 145-165.

LOCARNINI, R.A. 1994. *Water Masses and Circulation in the Ross Gyre and Environs*. PhD Thesis, Texas A&M University, 87 pp..

PICCO, P., AMICI, L., MELONI, R., LANGONE, L. & RAVAIOLI, M. 1999. Temporal variability of currents in the Ross Sea (Antarctica). In SPEZIE, G. & MANZELLA, G.M.R. eds. *Oceanogra-*

phy of the Ross Sea. Milano: Springer-Verlag, 103-118.

PILLSBURY, R.D. & JACOBS, S.S. 1985. Preliminary observations from long-term current meter moorings near the Ross Ice Shelf, Antarctica. In JACOBS, S.S. ed. *Oceanology of the Antarctic Continental Shelf*, Antarctic Research Series, **43**, 87-107.

ROCK, S.R. 1995. *Circulation and Heat Transport across the Ross Ice Shelf edge, Antarctica*. Master's Thesis, Lamont Doherty Earth Observatory of Columbia University, 37 pp. [Unpublished]

SMITH, W.H.F. & SANDWELL, D.T. 1997. Global Sea Floor Topography from Satellite Altimetry and Ship Depth Soundings. *Science*, **277**, 1956-1962.

TIMMERMANN, R., BECKMANN, A. & HELLMER, H.H. 2001. The role of sea ice in the freshwater budget of the Weddell Sea, Antarctica. *Annals of Glaciology*, **33**, 419-424.

TIMMERMANN, R., BECKMANN, A. & HELLMER, H.H. 2002. Simulation of ice-ocean dynamics in the Weddell Sea. Part I: Model configuration and validation. *Journal of Geophysical Research*, **107(C3)**, 10.1029/2000JC000471.

TIMMERMANN, R., HELLMER, H.H. & BECKMANN, A. 2002. Simulation of ice-ocean dynamics in the Weddell Sea. Part II: Interannual variability 1985-1993. *Journal of Geophysical Research*, **107(C3)**, 10.1029/2000JC000472.

TRUMBORE, S.E., JACOBS, S.S. & SMETHIE, W.M. Jr 1991. Chlorofluorocarbon evidence for rapid ventilation of the Ross Sea. *Deep Sea Research*, **38(7)**, 845-870.

ZOTIKOV, I.A. & JACOBS, S.S. 1985. Oceanic inclusions in the J-9 sea-ice core. *Antarctic Journal of the US*, **20(5)**, 113-115.

ZWALLY, H.J., COMISO, J.C. & GORDON, A.L. 1985. Antarctic offshore leads and polynyas and oceanographic effects. In JACOBS, S.S. ed. *Oceanology of the Antarctic Continental Shelf*, Antarctic Research Series, **43**, 203-226.

Figure captions

Fig.1. Model grid: **a.** Horizontal model grid in the Ross Sea sector including coast line (bold lines) and ice shelf mask (crossed boxes). Abbreviations: CA=Cape Adare, CC=Cape Colbeck, LAB=Little America Basin, Rv.Is.=Roosevelt Island, RI=Ross Island, McM.S.=McMurdo Sound. **b.** Vertical model layers on a section along 180°.

Fig.2. Modelled θ/S characteristics for the Ross Sea continental shelf (bottom depth < 1000m). Water masses in the ice shelf cavity are marked light grey: **a.** Summer. February 10-year mean. **b.** Winter. September 10-year mean. The diagram is supplemented by isopycnals (σ_0) and freezing temperature (T_f) relative to sea surface pressure. HSSW = High Salinity Shelf Water, LSSW = Low Salinity Shelf Water, ISW = Ice Shelf Water, MCDW = Modified Circumpolar Deep Water. Water mass definitions according to Trumbore et al. 1991.

Fig.3. 10-year mean horizontal circulation pattern in the Ross Sea. The thick yellow line marks the ice shelf edge: **a.** Bottom circulation. Velocities in the lowest model layer (vectors) and water column thickness (colour coded). **b.** Surface Circulation. Velocities (vectors) at the ocean surface in the open ocean and in the layer closest to the ice shelf base in the ice shelf cavity (Fig. 1b) and ice shelf draft (colour coded).

Fig.4. Modelled 10-year mean September sea ice conditions in the Ross Sea: **a.** Sea ice thickness distribution (grey-scale shaded area) and drift velocities (vectors). **b.** Sea ice growth rate (grey-scale shaded area) and NCEP wind velocities (vectors).

Fig.5. Section along the Ross Ice Shelf edge, facing south for salinity (colour coded) and density (thick, dashed contour lines): **a.** Summer. February 10-year mean. **b.** Winter. September 10-year mean, convectively adjusted and for meridional velocities. Positive values denote northward velocities, negative southwards. The ice shelf draft is marked by the thick, black, dashed line: **c.** Summer. February 10-year mean. **d.** Winter. September 10-year mean.

Fig.6. Seasonal variation of the vertically integrated transport (10-year mean). Shown is the vertically integrated transport stream function ψ : **a.** At maximum strength. 10-year mean for October. **b.** At minimum strength. 10-year mean for March. Solid contour lines / positive values denote cyclonic circulation cells, dashed contour lines / negative values anticyclonic ones.

Fig.7. Seasonal cycles of the circulation strength of the main anticyclonic circulation cell on the Ross Sea continental shelf as shown in Fig.6 (dashed line, upper left scale), ice shelf basal melt rate for the inner cavity (solid line, lower right scale) and mean potential temperature in the uppermost model layer in the inner cavity (dotted line, far left scale). Monthly mean values are shown and denoted by markers.

Fig.8. Distribution of basal melt rates under the Ross Ice Shelf (negative values and dashed contours denote freezing) and velocities in the uppermost model layer (vectors): **a.** Annual mean pattern. 10-year mean. **b.** December. 10-year mean. **c.** August. 10-year mean.

Fig.9. Mean annual cycle of monthly mean surface fresh-water fluxes from sea ice formation (dashed line), basal melting of the Ross Ice Shelf (including melting off the ice shelf edge, dotted line), net precipitation (grey line) and the overall total surface over the Ross Sea continental shelf (thick black line). Also shown is the sea ice transport off the Ross Sea continental shelf (thin solid line). 1 mSv = $10^3 \text{ m}^3 \text{ s}^{-1}$.

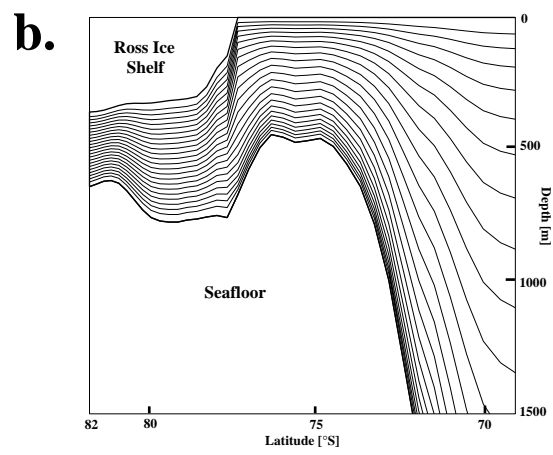
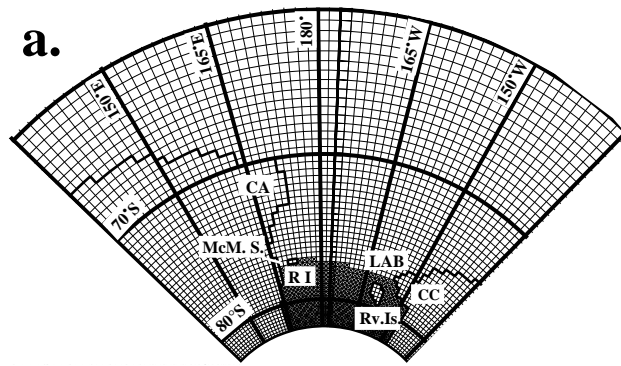


Fig.1

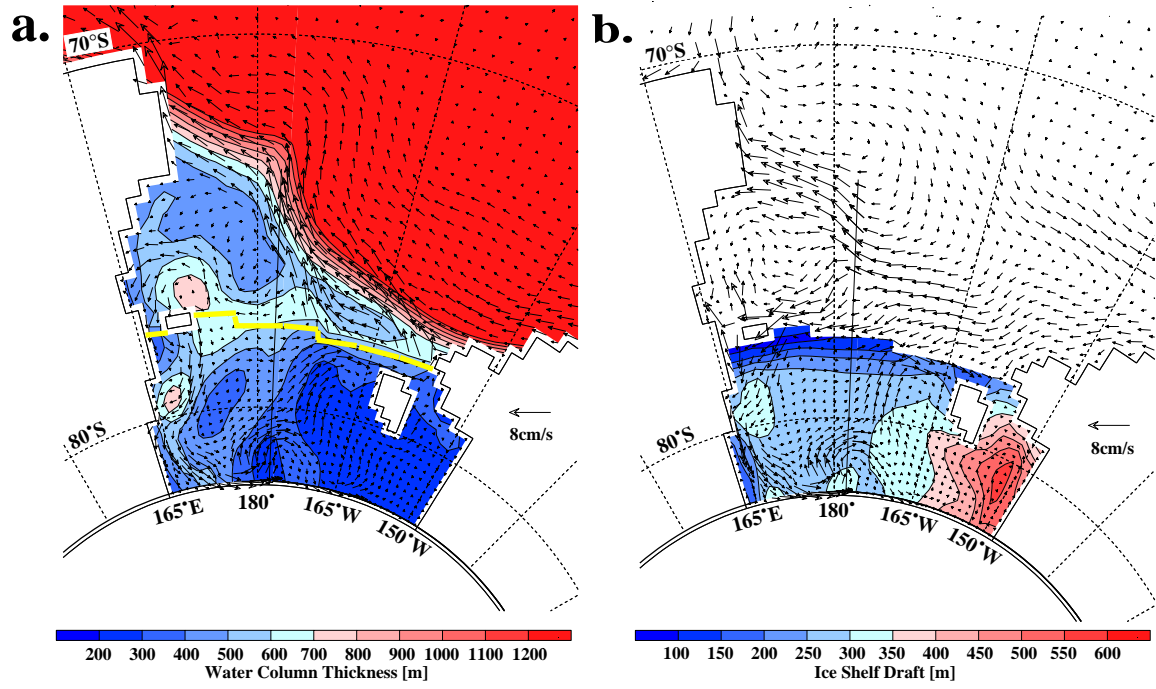


Fig.3

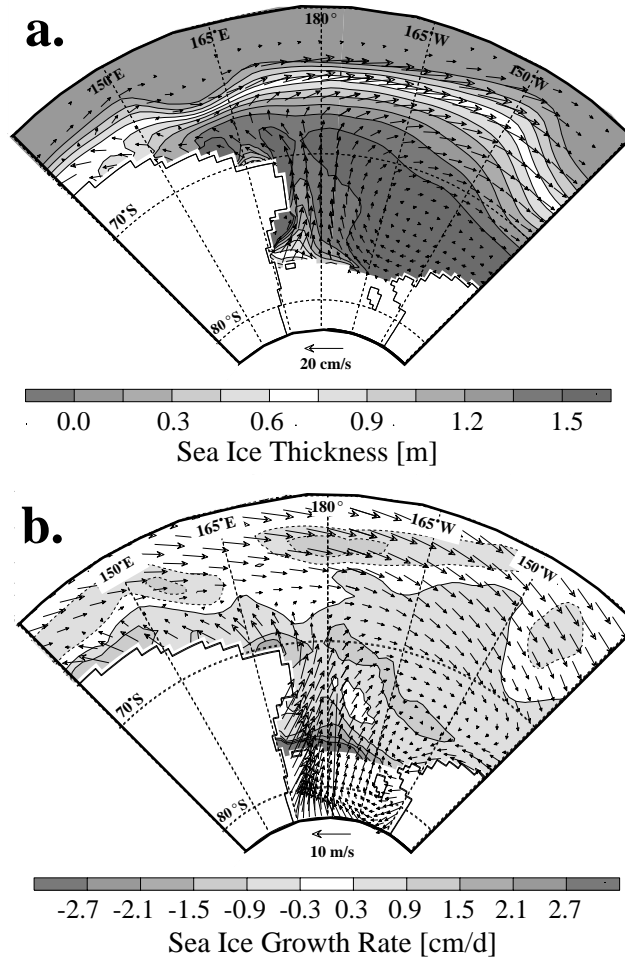


Fig.4

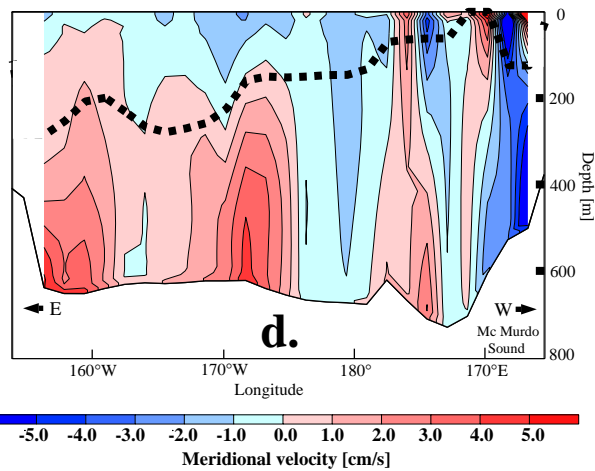
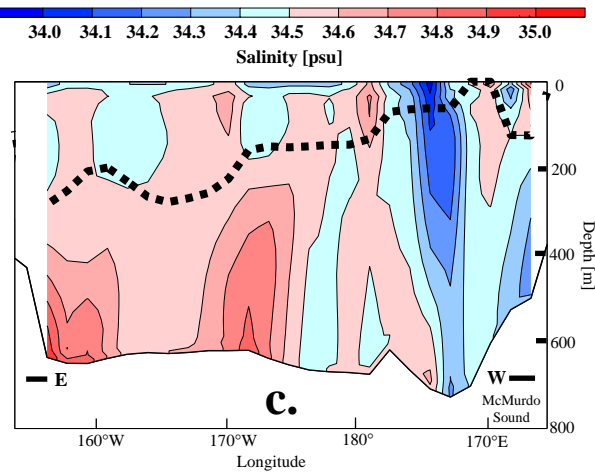
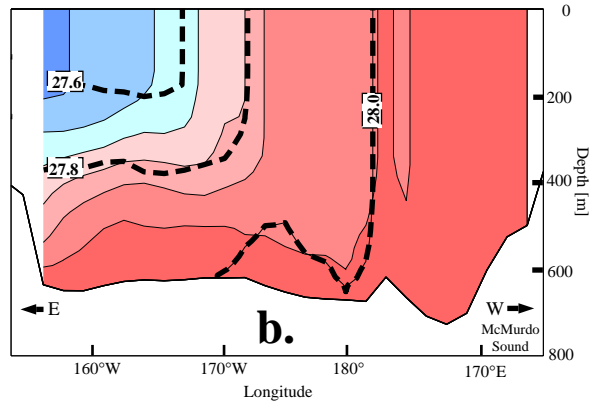
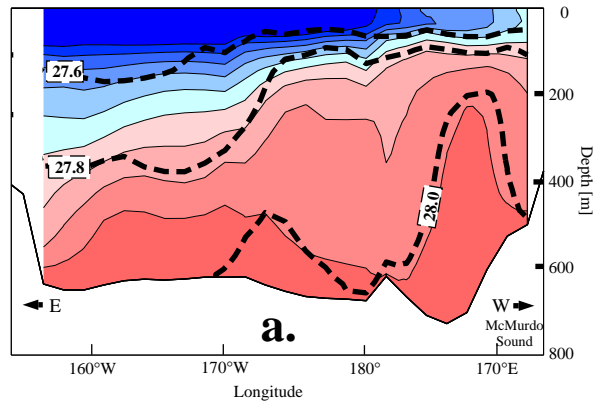


Fig.5

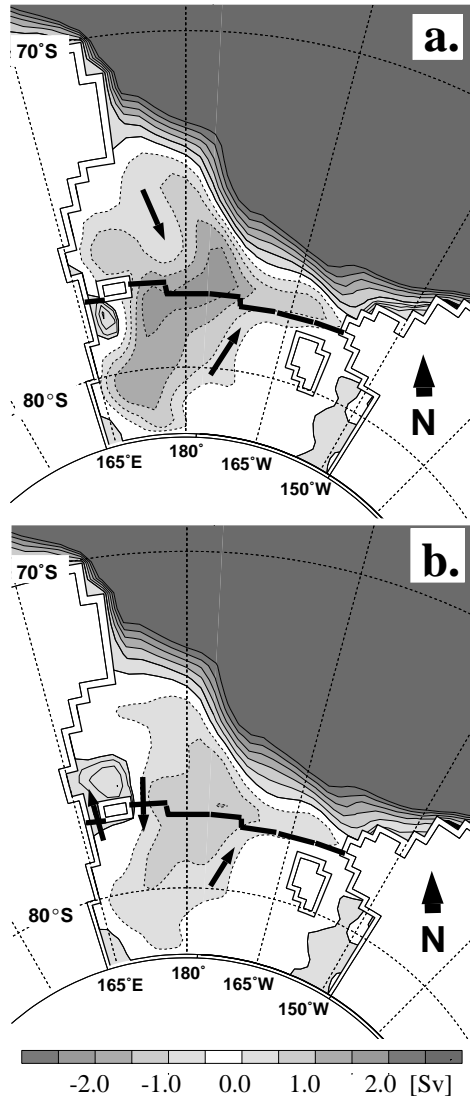


Fig.6

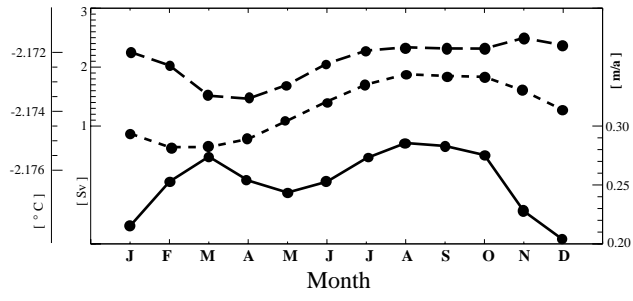


Fig.7

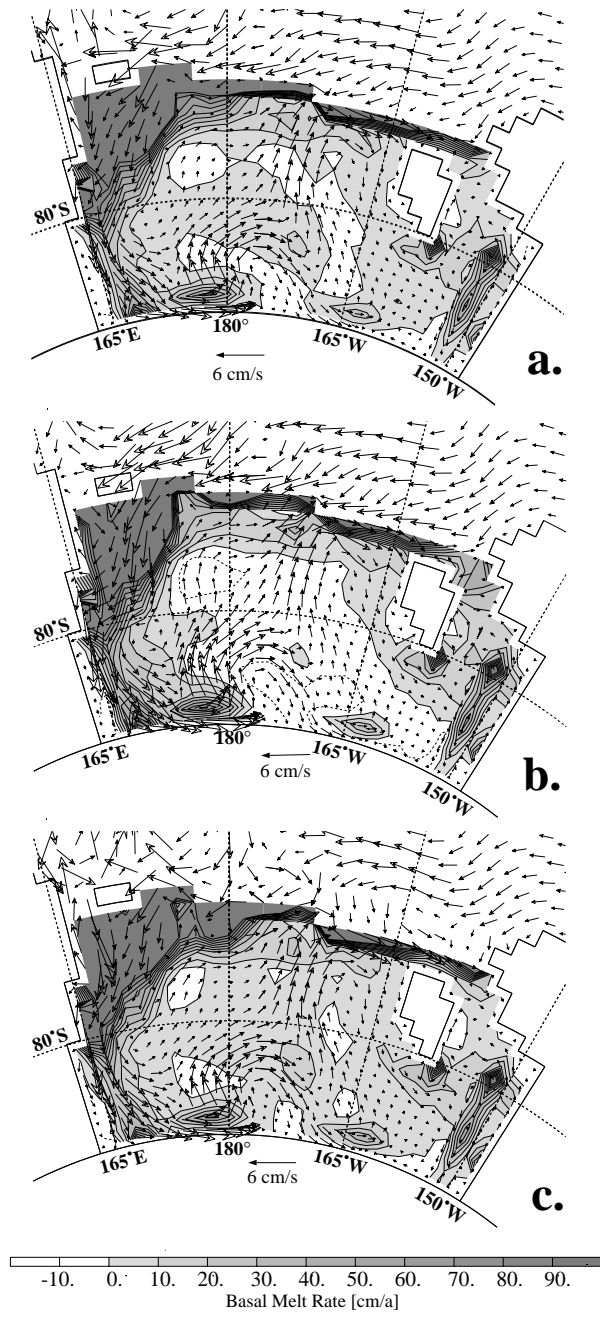


Fig.8

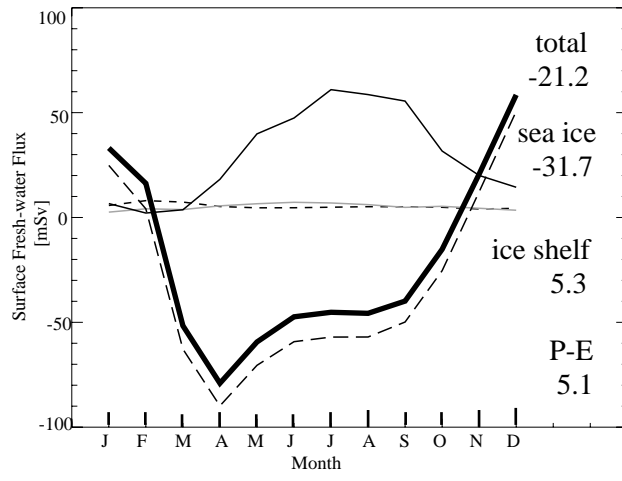


Fig.9